How a liquid becomes a glass both on cooling and on heating

Xinhui Lu,[1] S. G. J. Mochrie,[1,2] S. Narayanan,[3] A. R. Sandy,[3] and M. Sprung[3]

[1]*Department of Physics, Yale University, New Haven, Connecticut 06511*
[2]*Department of Applied Physics, Yale University, New Haven, Connecticut 06511*
[3]*Advanced Photon Source, Argonne National Laboratory, Argonne, IL 60439*

(Dated: February 4, 2008)

The onset of structural arrest and glass formation in a concentrated suspension of silica nanoparticles in a water-lutidine binary mixture near its consolute point is studied by exploiting the near-critical fluid degrees of freedom to control the strength of an attraction between particles and multispeckle x-ray photon correlation spectroscopy to determine the particles' collective dynamics. This model system undergoes a glass transition both on cooling and on heating, and the intermediate liquid realizes unusual logarithmic relaxations. How vitrification occurs for the two different glass transitions is characterized in detail and comparisons are drawn to theoretical predictions for glass formation in systems with attractive interactions.

The glass transition remains a grand challenge for condensed matter science [1, 2], with applications in diverse areas such as protein folding [3] and the flow of granular materials [4]. Especially remarkable then are predictions [5, 6, 7, 8], that in systems with short-ranged attractions a dense liquid may become a glass both on cooling and on heating. The scenario is as follows: When the ratio of attraction strength to temperature is small, the attractions play no role and, at high densities, a repulsion-dominated glass (RG) is realized [9, 10]. However, as the ratio is increased, surprisingly, attractions cause the glass to melt. With still further increase, the resultant liquid re-vitrifies into an attraction-dominated glass (AG). The intermediate liquid is itself highly unusual in that its density fluctuations are predicted to relax logarithmically in time. In the present paper, by exploiting fluid-mediated interactions between silica particles in a near-critical water-lutidine binary mixture to control the attraction strength [11, 12, 13], and multispeckle x-ray photon correlation spectroscopy (XPCS) [14, 15, 16] to determine the collective dynamics, we show that re-entrant glassy behavior and logarithmic relaxations are realized in this model system, simply by changing temperature. We are thus able to characterize in unprecedented detail how the non-ergodicity parameter of the RG decreases upon attraction-driven melting, and how relaxations in the intermediate fluid arrest as the attactive glass phase is approached.

Glassy states in colloidal suspensions are essentially spatially and temporally inhomogeneous [17, 18]. It is therefore paradoxical that mode-coupling theory (MCT) – a mean-field-like approach – is the only theory to-date capable of quantitative predictions concerning collective dynamics near the glass transition [10]. Nevertheless, MCT captures essential aspects of the dynamical arrest observed near the prototypical glass transition that occurs in a suspension of hard spheres [9, 10], where arrest occurs at sufficiently high densities, when each particle becomes trapped in a cage of its neighbours.

Instead of caging, it is intuitive that sufficiently strong interparticle attractions permit an alternate route to dynamical arrest, in which particles simply stick together. Recent MCT calculations carried out to investigate this possibility lead to the novel predictions of Refs. 5, 6, 7, 8. Support for these predictions comes from optical PCS experiments [19, 20, 21, 22], in which a depletion attraction between particles was created by the addition of non-adsorbing polymer. However, how the behavior evolves with attraction strength was only determined with limited resolution, in part because tuning the attraction requires laboriously mixing samples. By contrast, silica particles in near-critical water-lutadine (WL) mixtures experience a temperature-dependent attraction as a result of the confinement of the fluid critical fluctuations between particles [12], and evidenced by the particles' reversible aggregation as the temperature is increased towards the two-phase region [11]. Recently, Pontoni et al. [13] confirmed the temperature-dependent attraction via small-angle x-ray scattering (SAXS) and XPCS in a dilute sample. The present study was carried out to explore in detail how glassy behavior depends on attraction strength in *concentrated* suspensions of silica particles in near-critical WL mixtures.

Illustrated in Fig. 1(a) is the SAXS from 195 nm-radius silica spheres (polydispersity < 10%) at a volume fraction of $\phi \simeq 0.52$ in WL with a lutadine concentration of $c = 0.24$. Partially coherent illumination gives rise to a speckled intensity, whose mean and time-autocorrelation characterize the sample's static structure and dynamic relaxations, respectively. To this end, sequential SAXS patterns were collected using CCD-based area detectors at frame rates of up to 330 Hz (Run A and Run B) or 60 Hz (Run C) [16]. Fig. 1(b) shows the time and azimuthally averaged SAXS intensity (symbols) plotted versus wavevector (Q) in the neighbourhood of the peak in the interparticle structure factor, obtained at several temperatures during Run A. At the lowest temperature shown (33.400°C), there is a relatively narrow peak at $QR = 3.6$. With increasing temperature, the peak gradually becomes broader and shifts slightly toward larger QR, indicating a decrease in the correlation length, accompanied by slight decrease in the mean particle spacing. Concommitantly, the intensity increases for $QR \leq 2.5$, corresponding to the emergence of larger scale inhomogeneities. To quantify this evolution, we have fitted these data to the structure factor of spheres subject to a potential consisting of a hard core repulsion together with an attractive square well within the mean-spherical approximation [7]. The best fits – the solid lines in the figure – satisfactorily reproduce the main features of the data, especially in view of

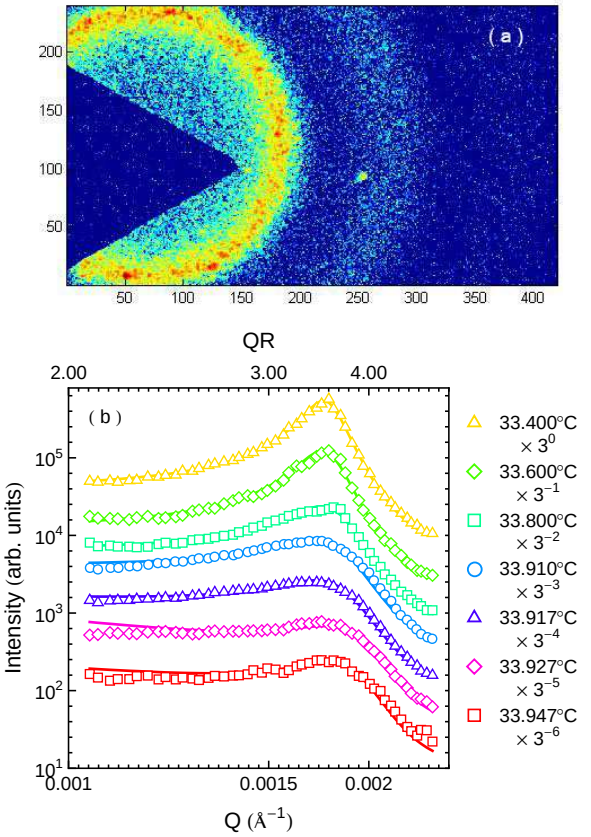

FIG. 1: (a) False-color image of the SAXS pattern from concentrated silica spheres in WL, obtained at beamline 8-ID at the Advanced Photon Source (APS) in Run A with a 0.15 s exposure. (b) Average SAXS intensity vs. wave vector obtained for several temperatures on warming (Run A). The lines are the best fits to the model described in the text.

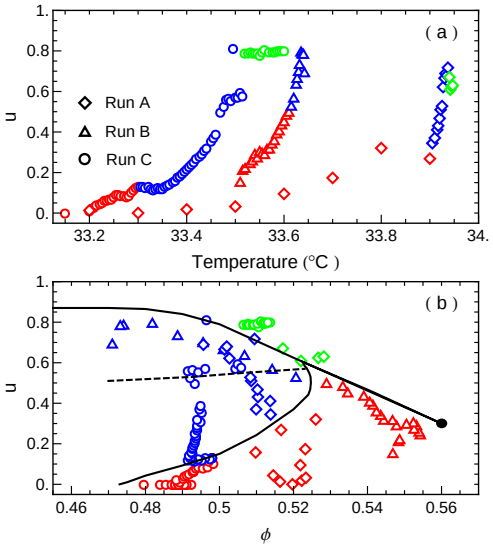

FIG. 2: (a) Best fit values of u for Run A (diamonds), B (triangles) and C (circles). The different colors indicate the different phases realized: red corresponds to a RG, blue to a liquid, and green to an AG. The fitted value of u appears constant in the AG, suggesting that no structural evolution occurs in this phase. (b) Phase diagram in the $u-\phi$ plane. Diamonds, triangles, and circles correspond to data points from Runs A, B, and C, respectively. Red, green, and blue symbols correspond to RG, AG, and liquid phases, respectively. Solid lines are schematic phase boundaries, inspired by Refs. 5, 6, 7, 8, with the black circle corresponding to the MCT A_3 singularity. The dashed line separates the region of logarithmic relaxations above the line, from the region of stretched exponential relaxations below. Although our particles are subject to gravitational settlement, the volume fraction across the height of the x-ray beam (20 μm) was approximately constant to within 1%. Usually, the volume fraction also remained constant in time. In Run B, however, the volume fraction varied as a result of slow settlement.

the fact that the only parameters varied in each fit were the overall intensity and the strength of the attraction (U). The particle radius and the hard core radius ($R = 200$ nm) were determined from fits to data obtained at the lowest temperature, where the attractive component is negligible. Because the model lineshape depends only on the dimensionless combination $u = U\Delta/(k_BTR)$ within the Q-range studied, the width (Δ) of the square-well attraction was fixed to be $0.01R$. At each temperature, the silica volume fraction was determined via the corresponding x-ray transmission of the sample. Fig. 2(a) shows the best fit values of u for run A (diamonds), and two additional warming runs: B (triangles) and C (circles). In each case, u takes on a small value at the lowest temperatures, but increases rapidly at a certain onset temperature. We ascribe the different onset temperatures for the different runs to small variations in the lutidine concentration between runs.

Normalized intermediate scattering functions (g_1) [16] at $QR = 2.34$ for delay times from 17 ms to 410 s for a sample with $\phi \simeq 0.49$ (Run C) are illustrated for temperatures from 33.000°C to 33.375°C in Fig. 3(a), and from 33.390°C to 33.600°C in Fig. 3(b). At the lowest temperature, g_1 shows an initial rapid decay (which is not fully captured by the 60 Hz frame rate of the camera employed in Run C) to reach a value of about 0.5 at 0.1 s. For times between 0.1 s and 100 s, g_1 remains nearly constant, revealing arrested dynamics over three decades in time. Such behavior is similar to that observed for hard-sphere glasses [9, 10] and is usually interpreted in terms of caging. The plateau value (f) is called the "non-ergodicity parameter". Because of the limited time range probed in the present study ($\lesssim 410$ s), we cannot determine whether the decrease in g_1 observed for times longer than about 200 s is a long-time equilibrium relaxation or is associated with aging of an arrested state [23]. As the temperature is increased, f decreases continuously to reach zero at 33.375°C [Fig. 3(a)], while the initial decay continues to about 0.3 s. Thus, within this range of tempertures, for which the interparticle attractions are increasing [Fig. 2(a)], remarkably, the initially-arrested RG melts into a dynamic liquid. The observed evo-

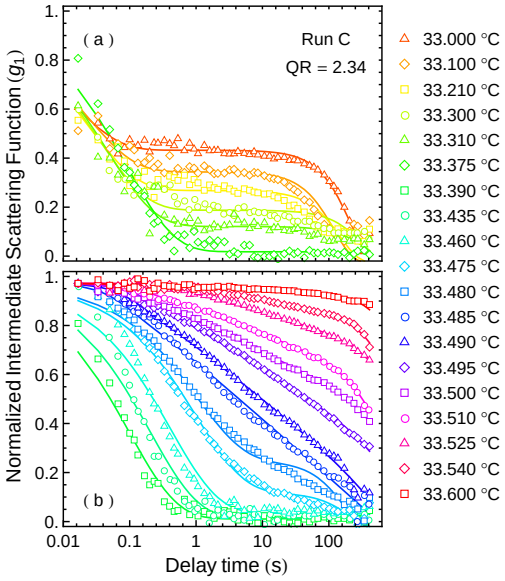

FIG. 3: g_1 versus delay time during Run C. For clarity, (a) corresponds to temperatures from 33.000°C to 33.375°C and (b) from 33.390°C to 33.600°C. Points are data. Lines correspond to the models discussed in the text.

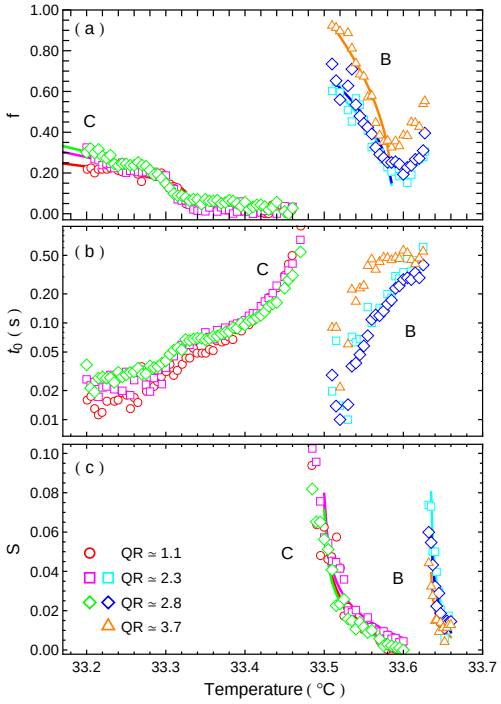

FIG. 4: (a) f, (b) t_0, and (c) S *vs.* temperature for Run B at $QR = 2.28$ (cyan squares), 2.86 (blue diamonds) and 3.70 (orange triangles), and for Run C at $QR = 1.13$ (red circles), 2.34 (magenta squares), and 2.82 (green diamonds). The solid lines are guides-to-the-eye.

lution of g_1 is distinct from what occurs when a hard sphere suspension undergoes the liquid-glass transition as a function of volume fraction. In that case, a plateau with a non-zero, Q-dependent value starts to emerge within the liquid phase, and, with further increase in the volume fraction, the plateau extends to longer times, showing only a small increase in its value through the glass transition [9, 10].

On warming beyond 33.375°C [Fig. 3(b)], the relaxation of g_1 becomes progressively slower with increasing temperature. On reaching 33.485°C, for times from about 0.1 s to about 100 seconds, g_1 appears nearly linear in the semi-log plot of Fig. 3(b), indicating the onset of nearly logarithmic relaxations. On warming still further, the logarithmic behavior continues, but with a slope that decreases with increasing temperature, so that by 33.600°C, g_1 barely decreases to 0.95 after 300 seconds, corresponding to an almost completely arrested state. As noted previously, logarithmic behavior of g_1 is expected for the liquid near an AG.

To quantify these observations, for temperatures from 33.000°C to 33.480°C, we have fitted g_1 using an empirical, modified-stretched-exponential form: $g_1 = \left[f + (1-f)e^{-(t/t_0)^{\alpha}}\right] e^{-(t/t_2)^{3/2}}$. To limit the number of parameters varied in the fits, the stretching exponent (α) was fixed to 0.6, leaving f, t_0 and t_2 as fitting parameters. From 33.485°C to 33.600°C, we have instead modeled g_1 via an alternate empirical form: $g_1 = \left[e^{-t/t_1} + (1-e^{-t/t_1})[1 - S\log(1+t/t_1)]\right] e^{-(t/t_2)^{3/2}}$, which manifests logarithmic relaxations for $t_2 \gg t \gg t_1$. On the semi-log axis of Fig. 3(b), S is the slope of the logarithmic g_1. In this case, the fitting parameters are S and t_2, while the onset of the logarithmic behavior (t_1) was fixed at 0.02 s. The solid lines in Figs. 3(a) and 3(b) correspond to the best fits to these models, providing a satisfactory account of the measured g_1 at all temperatures, except at 33.480°C, where g_1 is evolving from one form to the other. In both equations, the compressed exponential factor [23], involving t_2, accounts for the behavior at long times ($t_2 \geq 200$ s) and will not be discussed further in this paper.

Fig. 4(a) shows the best-fit values of f plotted versus temperature, obtained during run B at $QR = 2.28$, 2.86, and 3.70 and during Run C at $QR = 1.13$, 2.34, and 2.82. As may be seen, f takes a Q-dependent value with systematically larger values near the peak of the static structure factor ($QR \simeq 3.7$). This is similar to what is observed for hard-sphere glasses. However, here, f goes continuously to zero with increasing temperature. This behavior stands in contrast to what occurs at the melting of a hard-sphere glass with decreasing density, where the non-ergodicity parameter goes to zero discontinuously. MCT also predicts a discontinuous decrease in the non-ergodicity at the RG-to-liquid transition in the presence of attractive interactions [5, 6, 7]. Thus, this aspect of our measurements presents a contradiction to MCT. It may be noted, though, that certain MCT models [24] do permit a glass transition involving continuous increase in f as we ob-

serve in Run C. For Run B, density correlations relax very slowly, so that g_1 does not decrease to zero for times less than 200 s at any temperature. In fact, g_1 relaxes progressively more rapidly for temperatures increasing to 33.55°C, but relaxes progressively more slowly for temperatures increasing beyond 33.55°C. This leads to an apparent minimum in the fitted value of f at 33.55°C, before g_1 crosses over to the logarithmic form for 33.64°C and above. We ascribe the difference in behavior between Run B and Run C to the closer proximity of a glass-to-glass transition in Run B.

The best-fit values of the relaxation time (t_0) are shown in Fig. 4(b) plotted on a logarithmic scale versus temperature. Evidently, t_0 depends strongly on temperature. For both Runs B and C, t_0 increases rapidly with temperature from on the order of 0.02 s to reach about 0.5 s, before the relaxations become logarithmic. t_0 depends relatively weakly on Q, although in Run B it is somewhat larger at the structure factor peak ($QR = 3.7$) than elsewhere. For Run C, it was not possible to determine t_0 at the structure factor peak because of the presence of Bragg peaks from small coexisting crystallites. In comparison, a Q-independent time-scale, that increases rapidly with density, is a hallmark of relaxations near the glass transition of hard spheres.

The best-fit values of S within the logarithmic regime are summarized in Fig. 4(c) versus temperature. S is only weakly Q-dependent. Interestingly, near the temperature at which it vanishes, S appears to decrease approximately linearly to zero with increasing temperature. Although expressions for S are available within the context of MCT for small displacements in $u-\phi$ phase space from the so-called A_3 singularity point [24], it is unclear how these predictions relate to the behavior seen in Fig. 4(c).

Our results for the phase behavior of silica particles in WL in the volume fraction-interaction strength ($\phi - u$) plane are summarized in Fig. 2(b), where diamonds correspond to Run A, triangles to Run B, and circles to Run C. Each point is plotted with u determined by fitting the SAXS lineshape and with ϕ determined by the corresponding x-ray transmission. Red symbols correspond to the RG, defined for the purposes of the figure by the criterion that $g_1 > 0.17$ at $t = 10$ s. Green symbols correspond to the AG, defined similarly via $g_1 > 0.81$ at $t = 10$ *s*. Blue symbols correspond to the liquid. In the context of Refs. 5, 6, 7, 8, it is natural to add the schematic phase boundaries shown as solid lines in the figure. The dashed line in the figure separates the region of logarithmic relaxations above the line from the region of stretched exponential relaxations below. Overall, there is good agreement between our experimental phase diagram and that predicted. In addition, this study reveals a number of previously unremarked aspects including: (1) A continuous decrease in the non-ergodicity parameter with attraction strength through attraction-driven melting, (2) the existence of a weakly Q-dependent time-scale that increases through attraction-driven melting, and (3) the continuous decrease of S for temperatures increasing towards the liquid-to-attractive glass transition. We thank T. Chiba, E. R. Dufresne, R. L. Leheny, C. O'Hern, S. Sanis, M. Spannuth, M. Trias, and J. Wettlaufer for discussions, a referee for key clarifications, and the NSF for support via DMR 0453856. The APS is supported by the DOE.

[1] L.-M. Martinez and C. A. Angell, Nature **410**, 663 (2001).
[2] L. Berthier *et al.*, Science **310**, 1797 (2005).
[3] C. L. Brooks, J. N. Onuchic, and D. J. Wales, Science **293**, 612 (2001).
[4] A. J. Liu and S. R. Nagel, Nature **396**, 21 (1998).
[5] J. Bergenholtz and M. Fuchs, Phys. Rev. E **59**(5), 5706 (1999).
[6] L. Fabbian *et al.*, Phys. Rev. E **59**(2), R1347 (Feb 1999).
[7] K. Dawson *et al.*, Phys. Rev. E **63**, 011401 (2000).
[8] E. Zaccarelli *et al.*, Phys. Rev. E **66**(4), 041402 (2002).
[9] W. van Megen and P. N. Pusey, Phys. Rev. A **43**, 5429 (1991).
[10] W. Götze and L. Sjögren, Phys. Rev. A **43**, 5442 (1991).
[11] D. Beysens and D. Esteve, Phys. Rev. Lett. **54**, 2123 (1985).
[12] F. Schlesener, A. Hanke, and S. Dietrich, J. Stat. Phys. **110**, 981 (2003).
[13] D. Pontoni *et al.*, Phys. Rev. Lett. **90**, 188301 (2003).
[14] S. B. Dierker *et al.*, Phys. Rev. Lett. **75**, 449 (1995).
[15] S. G. J. Mochrie *et al.*, Phys. Rev. Lett. **78**, 1275 (1997).
[16] P. Falus, M. A. Borthwick, and S. G. J. Mochrie, Rev. Sci. Instr. **75**, 4383 (2004).
[17] E. R. Weeks *et al.*, Science **287**, 627 (2000).
[18] W. K. Kegel and A. van Blaaderen, Science **287**, 290 (2000).
[19] K. N. Pham *et al.*, Science **296**, 104 (2002).
[20] T. Eckert and E. Bartsch, Phys. Rev. Lett. **89**, 125701 (2002).
[21] H. S. Chen, W. R. Chen, and F. Mallamace, Science **300**, 619 (2003).
[22] K. N. Pham *et al.*, Phys. Rev. E **69**, 011503 (2004).
[23] R. Bandyopadhyay *et al.*, Phys. Rev. Lett. **93**, 228302 (2004). A compressed exponential is characteristic of an aging system.
[24] W. Götze and M. Sperl, Phys. Rev. E **66**(1), 011405 (2002).